

## THE POSSIBLE MOON OF KEPLER-90g IS A FALSE POSITIVE

D. M. Kipping<sup>1,2</sup>, X. Huang<sup>3</sup>, D. Nesvorný<sup>4</sup>,  
G. Torres<sup>1</sup>, L. A. Buchhave<sup>1,5</sup>, G. Á. Bakos<sup>3,6,7</sup>, A. R. Schmitt<sup>8</sup>

*Draft version July 22, 2018*

### ABSTRACT

The discovery of an exomoon would provide deep insights into planet formation and the habitability of planetary systems, with transiting examples being particularly sought after. Of the hundreds of *Kepler* planets now discovered, the seven-planet system Kepler-90 is unusual for exhibiting an unidentified transit-like signal in close proximity to one of the transits of the long-period gas-giant Kepler-90g, as noted by Cabrera et al. (2014). As part of the “*Hunt for Exomoons with Kepler*” (HEK) project, we investigate this possible exomoon signal and find it passes all conventional photometric, dynamical and centroid diagnostic tests. However, pixel-level light curves indicate that the moon-like signal occurs on nearly all of the target’s pixels, which we confirm using a novel way of examining pixel-level data which we dub the “*transit centroid*”. This test reveals that the possible exomoon to Kepler-90g is likely a false positive, perhaps due to a cosmic ray induced Sudden Pixel Sensitivity Dropout (SPSD). This work highlights the extreme care required for seeking non-periodic low-amplitude transit signals, such as exomoons.

*Subject headings:* techniques: photometric — stars: individual (Kepler-90) — planets and satellites: general — planetary systems

### 1. INTRODUCTION

The discovery of a confirmed extrasolar moon remains an outstanding challenge to modern astronomy. Despite nearly 2000 exoplanets having now been discovered (www.exoplanet.eu; Schneider et al. 2011), with some smaller than Mercury (Barclay et al. 2013), the confirmed existence of a satellite to any of these planets eludes us.

Both gravitational microlensing and transit photometry are predicted to be sensitive to “large” exomoons (masses  $\gtrsim 0.1 M_{\oplus}$ ) and yet even a plausible candidate system remains elusive. As an example of the sensitivity from microlensing, Bennett et al. (2014) recently identified a system (MOA-2011-BLG-262Lb) which is either composed of a Neptune orbiting a late M-dwarf or a terrestrial moon ( $\sim 0.5 M_{\oplus}$ ) orbiting a super-Jupiter, with the moon scenario statistically disfavored<sup>9</sup>. Using transits, our project (the “*Hunt for Exomoons with Kepler*”; HEK) has published exomoon constraints for 17 transiting planets with six yielding sub-Earth mass constraints (Kipping et al. 2013a,b, 2014).

Recently, Cabrera et al. (2014) and Schmitt et al. (2014) announced the discovery of the first example of

a seven-planet transiting system, Kepler-90 (KOI-351). Notably, Cabrera et al. (2014) discuss the possibility of the 210.6 d period planet, Kepler-90g, hosting a large exomoon, largely driven by a moon-like transit signal neighboring the third transit of this gas giant. Although Cabrera et al. (2014) remained cautious and did not claim to have found the first exomoon candidate, the visually apparent moon-like signal remains a mystery and arguably the most plausible evidence for a transiting exomoon in the published literature. For this reason, as part of the on-going HEK project, we here present an investigation of the possible exomoon of Kepler-90g, dubbed Kepler-90g.01 in what follows.

### 2. PHOTOMETRIC ANALYSIS

#### 2.1. Background

We begin our investigation by exploring whether the full set of photometric observations of Kepler-90g can be explained by a planet-moon configuration, which was not attempted by Cabrera et al. (2014). There are two reasons why one might suspect this is not possible. Firstly, there is apparently only one high-significance piece of evidence for Kepler-90g.01, namely the companion transit to Kepler-90g in Q6 (quarter 6), as shown in Fig. 1. This raises the question as to whether it is dynamically possible for Kepler-90g.01 to avoid imparting a second transit elsewhere for the other five transits of Kepler-90g. Secondly, the transit of Kepler-90g.01 is  $\sim 21.5$  hours later than that of Kepler-90g, implying a large planet-moon separation. Indeed, this is the principal reason why Cabrera et al. (2014) do not consider the moon hypothesis likely, arguing the moon would be on the edge of Hill stability.

#### 2.2. Data Treatment

The seven-planet system, Kepler-90, was observed continuously by the *Kepler* spacecraft from Q1 to Q17, ex-

arXiv:1411.7028v1 [astro-ph.EP] 25 Nov 2014

<sup>1</sup> Harvard-Smithsonian Center for Astrophysics, Cambridge, MA 02138, USA; email: dkippping@cfa.harvard.edu

<sup>2</sup> Cfa Menzel Fellow

<sup>3</sup> Dept. of Astrophysical Sciences, Princeton University, Princeton, NJ 05844, USA

<sup>4</sup> Dept. of Space Studies, Southwest Research Institute, 1050 Walnut St., Suite 300, Boulder, CO 80302, USA

<sup>5</sup> Centre for Star and Planet Formation, Natural History Museum of Denmark, University of Copenhagen, DK-1350 Copenhagen, Denmark

<sup>6</sup> Alfred P. Sloan Fellow

<sup>7</sup> Packard Fellow

<sup>8</sup> Citizen Science

<sup>9</sup> We define a “candidate” exomoon to be a case where the moon hypothesis is favored but it has not been unambiguously demonstrated to be uniquely explained by said hypothesis.

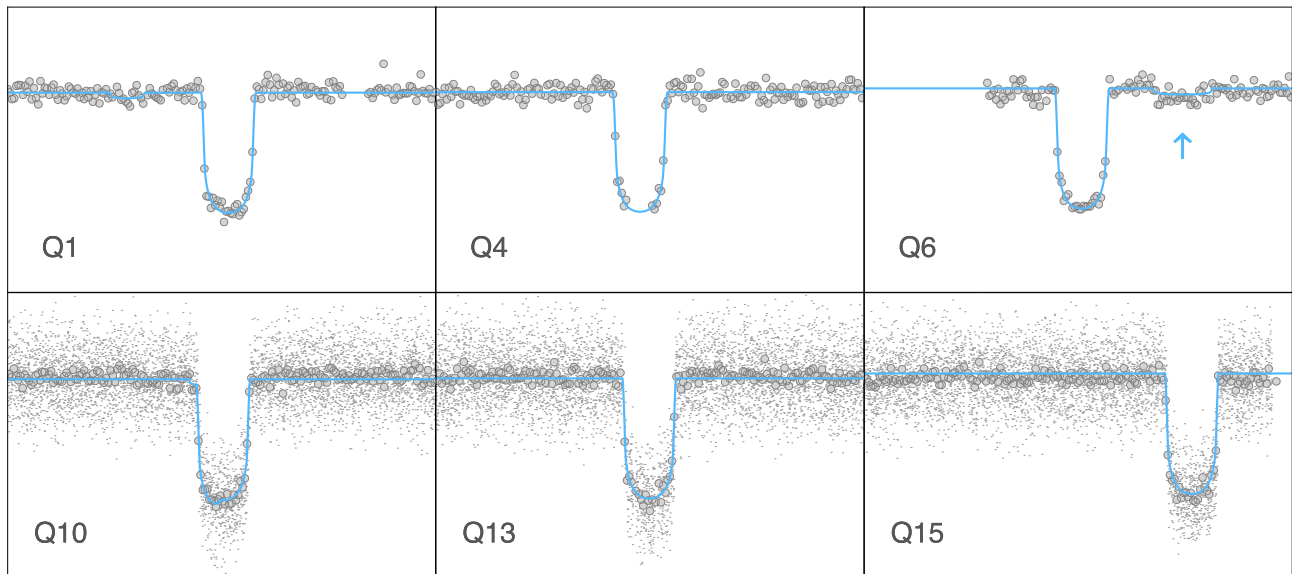


FIG. 1.— Photodynamical light curve fit (solid line) of the six transits of Kepler-90g, including an exomoon and freely fitted transit times. Filled circles represent the LC data, and dots represent the SC data (where available). Temporal baseline (x-axis) of each caption is 96 hours, centered on the times of transit minimum for a linear ephemeris. Relative flux (y-axis) plotted from 0.993 to 1.003. The Kepler photometry of Kepler-90g is well-explained by an exomoon plus additional TTVs.

cept for Q8, Q12 and Q16 where the target fell off the CCDs. We use all of the available data for this target, including the short-cadence observations where available (from Q9 onwards). The Pre-search Data Conditioning (PDC) time series (Smith et al. 2012) was downloaded and detrended after first excluding all transits, outliers and manually removing discontinuities (e.g. ramps), in the same way described in our previous papers (e.g. see Kipping et al. 2014). Long-term detrending for the transit photometry of Kepler-90g was handled by the CoFIAM algorithm (Kipping et al. 2013a), protecting timescales less than or equal to the full duration of Kepler-90g (12.593 hours; Table 3 of Cabrera et al. 2014).

Kepler-90g exhibits a  $\sim 1$  day transit timing variation (TTV) for its sixth and final transit, which is far too large to be due to an exomoon alone (Kipping 2009). For this reason, we model the six transits of Kepler-90g using the photodynamical planet-moon code LUNA (Kipping 2011) plus six freely fitted transit times, which are likely due to planet-planet interactions. By fitting the transit times freely, any TTVs due to an exomoon are absorbed by these parameters and thus would be degenerate with the moon’s mass. This is particularly salient since TTVs due to an exomoon should dominate a mass determination over transit duration variations (TDVs; Kipping 2009), due to the visually obvious large separation between the transits of Kepler-90g and Kepler-90g.01, implying a large planet-moon separation. For these reasons, the mass of the exomoon is simply set to zero in the photodynamical model (but the moon radius is still freely fitted). As with our previous works, we regress our model to the detrended photometry using the MULTINEST package (Feroz et al. 2008, 2009), with our priors following those of Kipping et al. (2014).

### 2.3. Results: Formal Significance

Using the Bayesian evidence computed by MULTINEST, we find a planet+moon+TTVs model is favored

over a planet+TTVs model with a formal significance of  $5.2\sigma$  ( $\Delta \ln \mathcal{Z} = 15.3 \pm 0.2$ ). Furthermore, we find that the six transits of Kepler-90g are well-explained by this model, with Kepler-90g.01 imparting two dominant signals on the light curve, the originally identified signal during Q6 and a second event preceding the first transit of Kepler-90g (Q1), as shown in Fig. 1.

The Q6 transit of Kepler-90g.01 is supported by a change in  $\chi^2$  of  $\Delta\chi^2 = 49.0$  over 26 data points. The Q1 transit is far less convincing, imposing a modest improvement of  $\Delta\chi^2 = 11.1$  over 15 data points, during a period of increased light curve scatter. We also note a very minor exomoon feature during the Q10 transit of negligible significance. We therefore conclude that the case for Kepler-90g.01 rests solely on the reality of the Q6 moon-like transit.

### 2.4. Results: Plausibility of Parameters

The parameters for the planet-moon system, assuming  $R_\star = (1.2 \pm 0.1) R_\odot$  (Cabrera et al. 2014), indicate a  $(7.96 \pm 0.65) R_\oplus$  planet orbited by  $(1.88 \pm 0.21) R_\oplus$  exomoon at semi-major axis of  $(a_{SP}/R_P) = 69.4_{-6.4}^{+7.3}$  planetary radii. We find short-period moons ( $\lesssim 10$  days) are prohibited, but otherwise the moon’s period posterior distribution is broad, leading to a wide range of possible planet-densities via the technique described in Kipping (2010) of  $\rho_P < 21.4 \text{ g cm}^{-3}$  to 95% confidence. In the case of Kepler-90g, a more useful constraint on the planet’s density comes from demanding the moon orbit within the Hill sphere, which requires

$$\left(\frac{M_P}{M_\star}\right) > 3 \left(\frac{(R_P/R_\star)(a_{SP}/R_P)}{(a/R_\star)}\right)^3, \quad (1)$$

where the bracketed terms on the right-hand side are all observables from our light curve model. Using our posterior distributions, this constraint imposes

$(M_P/M_\star) > (8.4^{+3.1}_{-2.1}) \times 10^{-5}$ . Dynamically speaking, we estimate the seven-planet system is stable if Kepler-90g has a mass  $(M_P/M_\star) \lesssim 2 \times 10^{-4}$ , implying the Hill sphere can plausibly extend to encompass this moon signal.

Since  $\rho_P = \rho_\star(M_P/M_\star)(R_P/R_\star)^{-3}$ , then our limit may be expressed as  $\rho_P > 0.39^{+0.14}_{-0.10} \text{ g cm}^{-3}$ , where we have used  $\rho_\star = (1.036 \pm 0.033) \text{ g cm}^{-3}$ , based on averaging the light curve derived stellar densities from the seven planets in the system. Densities greater than this sub-Saturn mean density are certainly plausible for an  $8 R_\oplus$  planet. Additionally, for a retrograde moon, Domingos et al. (2006) argue moons are stable up to nearly the edge of the Hill sphere ( $\sim 93\%$ ).

### 2.5. Conclusions

Based on our light curve analysis, we draw the following conclusions. Firstly, the light curve can be well-explained by Kepler-90g hosting a single large exomoon. Although the formal significance is  $5.2\sigma$ , we find that the significance is dominated by the single moon-like transit in Q6, which indicates the need for a careful inspection of this event. Secondly, we find that Kepler-90g.01 can be within the Hill sphere of the Kepler-90g, if Kepler-90g has a mean density in the range of  $0.39 \rightarrow 0.93 \text{ g cm}^{-3}$  (upper limit based on seven-planet stability), which is certainly plausible given the radius of  $8 R_\oplus$ .

## 3. CENTROID ANALYSIS

### 3.1. Conventional Centroids

We have now established that the case for an exomoon around Kepler-90g now rests solely on the reality of the Q6 moon-like transit. The usual detection criteria used by the HEK project (Kipping et al. 2013a) are less useful for this system, since for example we cannot conduct double-likelihood tests by omitting some of the transits, given that there is just one moon-like signal. Low amplitude transit-like events are sometimes imparted into the *Kepler* time series due to various sources of false positives, ranging from astrophysical to instrumental (Tenenbaum et al. 2014).

We confirmed that this signal is coherent in both the PDC and Simple Aperture Photometry (SAP) data products, using both CoFIAM and polynomial detrendings of each. The moon-like signal is therefore not an artifact of the PDC pipeline, which can occur in rare instances (Christiansen et al. 2013). Using the Pixel Response Function (PRF; see Bryson et al. 2010), precise centroids of each *Kepler* target are made available as a standard data product. These may be used to identify certain types of false positive scenarios, such as a background eclipsing binary, and this has become a standard component of the Data Validation (DV) process by the *Kepler* team (Bryson et al. 2013). During a transit, a large centroid shift indicates that the true eclipsing object is offset from the total flux centroid.

In Fig. 2, we show the time series of the  $x$  (column) and  $y$  (row) centroids for Kepler-90 during Q6, after detrending with CoFIAM. The highlighted areas depict the times when Kepler-90g and Kepler-90g.01 are transiting. Both signals appear reasonably consistent with the out-of-transit centroids at a level  $< 3\sigma$  (the typical threshold in DV reports). We find no compelling reason to reject the possible moon Kepler-90g.01 based on this informa-

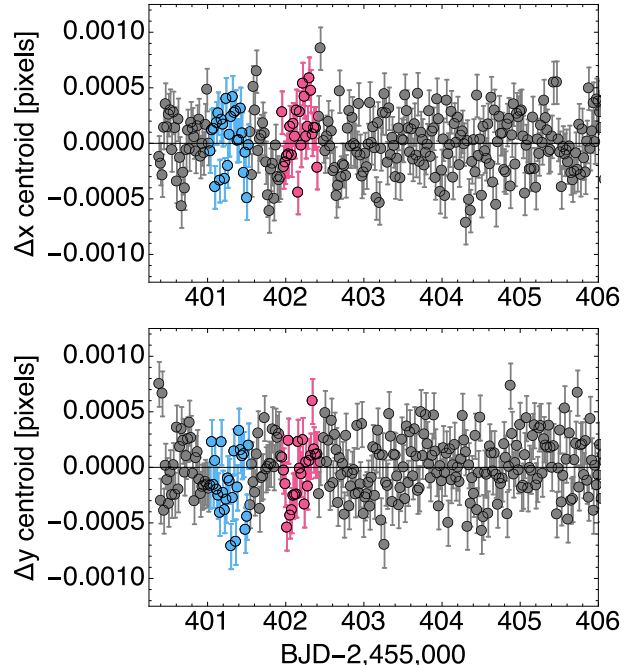


FIG. 2.— Time series of Kepler-90’s centroids around the time of Kepler-90g’s transit in Q6. Blue points are those occurring during the transit of Kepler-90g and pink are those occurring during the transit of the putative exomoon Kepler-90g.01.

tion.

### 3.2. “Transit Centroids”

We wished to understand where on the CCD the transits occur and how localized the transit signals were relative to the point spread function. In order to investigate this, we considered a new type of centroid we dub the “transit centroid”. Whereas a conventional centroid calculates the mean pixel position weighted by the flux of each pixel, the transit centroid instead weights by the signal-to-noise ratio (SNR) of the transit depth on each pixel. Since the flux drops away from the flux centroid, causing greater photon noise, the SNR should be located at the same position as the flux centroid. If high SNR transits are found far away from the flux centroid, this is an indication that the transit is not localized at the expected flux centroid position. We define the transit centroid position as:

$$x_{\text{transit}} = \frac{\sum_{i=1}^N x_i (\delta_i / \sigma_i)}{\sum_{i=1}^N (\delta_i / \sigma_i)} \quad (2)$$

$$y_{\text{transit}} = \frac{\sum_{i=1}^N y_i (\delta_i / \sigma_i)}{\sum_{i=1}^N (\delta_i / \sigma_i)}, \quad (3)$$

where  $\{x_i, y_i\}$  is the Cartesian location of the center of the  $i^{\text{th}}$  pixel,  $\delta_i$  is the transit depth recorded on that pixel and  $\sigma_i$  is the associated uncertainty on that transit depth. For the depth calculation, we simply compute the mean flux within the durations found by our earlier photodynamical fits and use the standard error as the uncertainty.

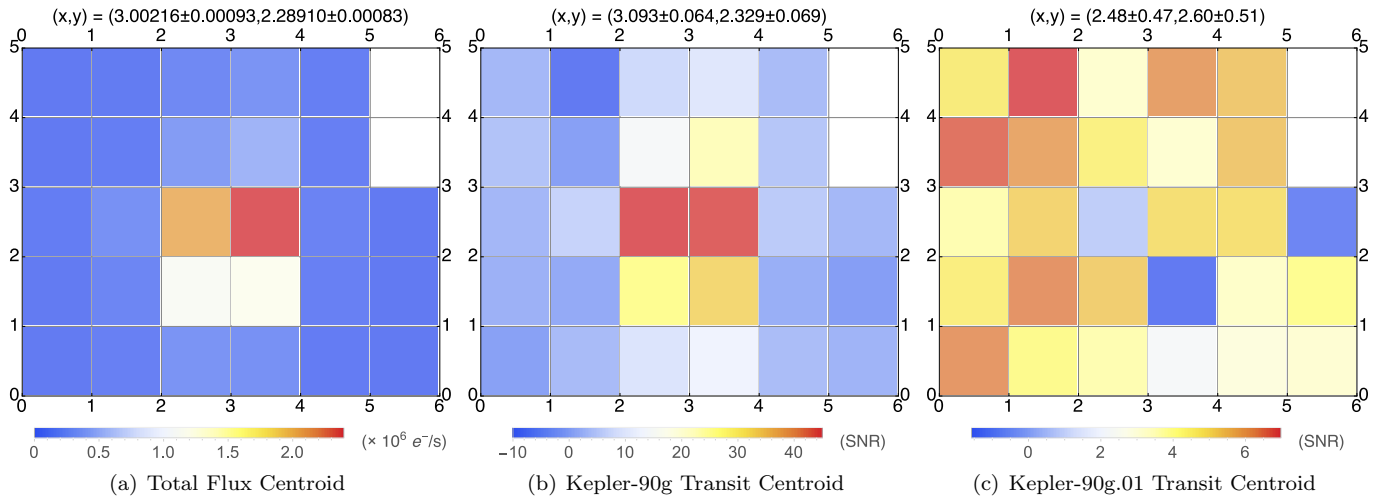


FIG. 3.— Kepler pixel map of Kepler-90 during Q6. From blue to red, the color of each pixel is proportional to the signal-to-noise of the transit signal identified in this quarter, except for panel a) where the color scales with the flux. Kepler-90g.01 displays a highly delocalized transit centroid, making it doubtful as signal of astrophysical origin.

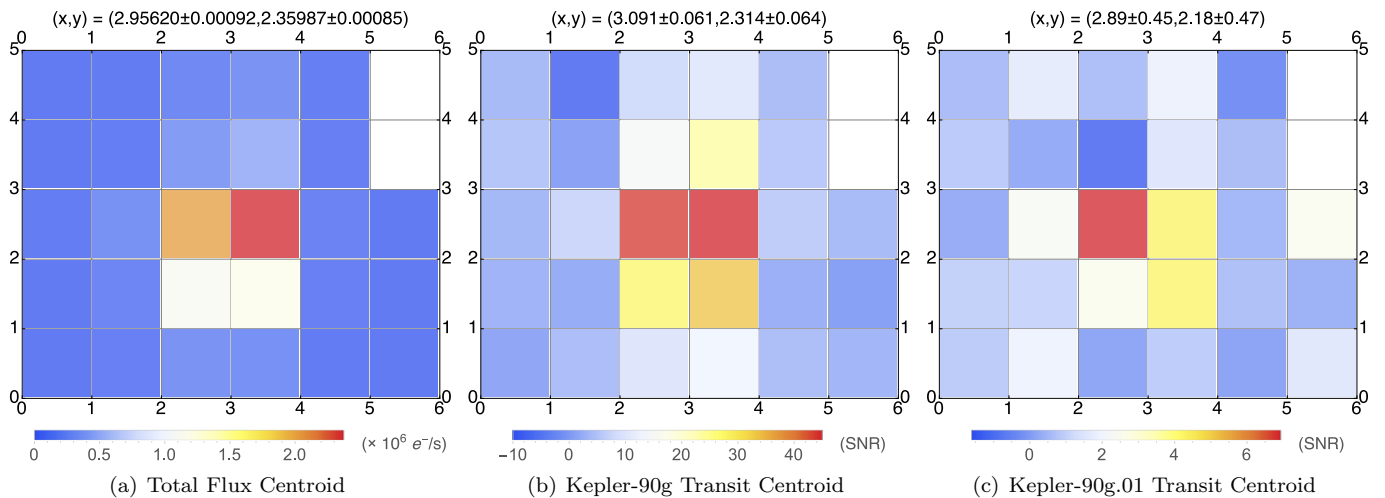


FIG. 4.— Same as Fig. 3, except we have replaced the moon candidate with an injected fake moon of equivalent transit depth. Unlike the real data, the Kepler-90g.01 transit centroid is localized at the center of the postage stamp, along with the Kepler-90g and the total flux.

The SNR of each pixel for the transits of Kepler-90g and Kepler-90g.01 during Q6 are color coded on Fig 3(b) & 3(c) respectively, which may be compared to the total flux centroid shown in Fig. 3(a). Centroid positions are provided at the top of each panel in Fig 3, with uncertainties estimated using a bootstrap of each pixel’s light curve residuals. Although the Kepler-90g.01 transit centroid is not significantly offset ( $< 2\sigma$ ) from the planetary transit, the SNR pattern for Kepler-90g.01 is quite distinct. Specifically, it is clear that the moon-like signal is not localized at the center of the postage stamp, unlike Kepler-90g, with even pixels on the edges showing high SNR levels.

We considered the possibility that the fact Kepler-90g.01 is such a low amplitude transit is responsible for the transit centroid’s delocalization, i.e. the data are not good enough to pin down the location. To test this, we created a fake Q6 time series by taking the pixel-level light curves of Kepler-90g’s transit, reducing the depth to equal that of Kepler-90g.01, and injecting it in place of the original Kepler-90g.01 transit for each pixel. Since

the durations of the events are similar (12.1 hours for g and 10.4 hours for g.01), this process should produce a realistic estimate of the transit centroid pattern produced if Kepler-90g.01 were a genuine exomoon. Recalculating the transit centroids (see Fig. 4), we find that of the fake moon to be highly localized, as visible in Fig. 4(c), and the transit centroid is now within  $1\sigma$  of both Kepler-90g and the total flux. This test indicates that the delocalized structure seen in Fig. 3(c) is strong evidence that the Kepler-90g.01 transit is spurious.

On this basis, we identify Kepler-90g.01 as a false positive exomoon. The underlying origin for the anomalous transit centroid is unclear, but may be due to a cosmic ray hit causing Sudden Pixel Sensitivity Dropout (SPSD) at this time (see Christiansen et al. 2013). As a further check, we tried detrending the Q6 photometry using the Trend Filtering Algorithm (TFA) described in Huang et al. (2013), which searches for common mode behaviors on the same CCD module. We find that the moon-like transit persists in the TFA light curve, indicating that the other stars on this module do not exhibit

the event. For the purposes of this short letter it is unimportant what the actual origin is; the key conclusion is that the signal is unlikely to be that of an exomoon.

#### 4. DISCUSSION

In this work, we have demonstrated that the exomoon-like transit signal identified near one of the transits of the  $8 R_{\oplus}$  exoplanet Kepler-90g by Cabrera et al. (2014) is likely a false positive. This determination is far from obvious, having required us to introduce a new tool to examine *Kepler* pixel-level data.

Cabrera et al. (2014) originally suggested the signal may be spurious based on the large temporal separation between the transit of Kepler-90g and the moon-like transit. However, in this work, we find that the separation corresponds to a moon within the Hill sphere, provided Kepler-90g has a mean density exceeding  $0.39 \text{ g cm}^{-3}$ . Further, a retrograde exomoon would be stable up to nearly the edge of the Hill sphere, following Domingos et al. (2006). Based on dynamical stability simulations, the seven-planet system in which Kepler-90g resides is stable provided g has a density below  $0.93 \text{ g cm}^{-3}$ . Finally, we find that the fact that only one of the six observed transits of Kepler-90g shows a high signal-to-noise exomoon transit is easily explained with a photodynamical model. Based on a purely photometric analysis then, one would conclude that this is a plausible exomoon candidate.

Analysis of the PRF centroids shows no significant deviations during the times of Kepler-90g's transit, nor that

of the moon-like signal. Inspecting the pixel-level data however, we suspected that the moon-like transits were occurring on nearly all pixels rather than being centered on the flux centroid. To test this, we considered a new test, dubbed the “transit centroid”, which computes a centroid position weighted by the signal-to-noise of the transit, as seen by each pixel. This test confirms that the moon-like transit is not localized at the expected position, a result which we demonstrate is not due to the low amplitude nature of the moon-like signal either. We conclude that the moon-like transit is likely an instrumental artifact, perhaps due to a cosmic ray causing a Sudden Pixel Sensitivity Dropout (Christiansen et al. 2013).

This work establishes that the moon-like signal near Kepler-90g is likely spurious and does not constitute compelling evidence for a transiting exomoon. The fact that the candidate passes all of the conventional tests, such as photodynamical modeling, imposing dynamical stability and centroid analysis, highlights the extreme difficulty facing exomoon hunters, due to the non-periodic and low-amplitude nature of the signals being sought. Nevertheless, the sensitivity to sub-Earth mass exomoons using *Kepler* is firmly established and despite the mine-field of false positives, a confirmed detection is surely inevitable.

#### ACKNOWLEDGEMENTS

This work made use of the Michael Dodds Computing Facility. DMK is funded by the CfA Menzel Fellowship. GB acknowledges partial support from NSF grant AST-1108686 and NASA grant NNX12AH91H.

#### REFERENCES

- Barclay, T., Rowe, J. F., Lissauer, J. J., et al., 2013, *Nature*, 494, 452
- Bennett, D. P., Batista, V., Bond, I. A., et al., 2014, *ApJ*, 785, 155
- Bryson, S. T., Tenenbaum, P., Jenkins, J. M., et al., 2010, *ApJ*, 713, L97
- Bryson, S. T., Jenkins, J. M., Gilliland, R. L., et al., 2013, *PASP*, 125, 889
- Cabrera, J., Csizmadia, Sz., Lehmann, H. et al., 2014, *ApJ*, 781, 18
- Christiansen, J. L., Clarke, B. D., Burke, C. J., et al., 2013, *ApJS*, 207, 35
- Domingos, R. C., Winter, O. C. & Yokoyama, T., 2006, *MNRAS*, 373, 1227
- Feroz, F. & Hobson, M. P., 2008, *MNRAS*, 384, 449
- Feroz, F., Hobson, M. P. & Bridges, M., 2009, *MNRAS*, 398, 1601
- Huang, X., Bakos, G. A. & Hartman, J. D., 2013, *MNRAS*, 429, 2001
- Kipping, D. M., 2009, *MNRAS*, 392, 181
- Kipping, D. M., 2010, *MNRAS*, 409, L119
- Kipping, D. M., 2011, *MNRAS*, 416, 689
- Kipping, D. M., Hartman, J., Buchhave, L. A., et al., 2013a, *ApJ*, 770, 101
- Kipping, D. M., Forgan, D., Hartman, J., et al., 2013b, *ApJ*, 777, 134
- Kipping, D. M., Nesvorný, D., Buchhave, L. A., et al., 2014, *ApJ*, 784, 28
- Schmitt, J. R., Wang, J., Fischer, D. A., et al., 2014, *AJ*, 148, 28
- Schneider, J., Dedieu, C., Le Sidaner, P., Savalle, R. & Zolotukhin, I., 2011, *A&A*, 532, 79
- Smith, J. C., Stumpe, M. C., Van Cleve, J. E., et al., 2012, *PASP*, 124, 1000
- Tenenbaum, P., Jenkins, J. M., Seader, S., et al., 2014, *ApJS*, 211, 6